JET–R(97)01

Recent Advances in Relability and Life Predictions of Critical JET Neutral Beam Components based on Realistic Material Data for DTE1 Operation and possible Upgraded Injector Scenarios

S Papastergiou.

JET Joint Undertaking, Abingdon, Oxfordshire, OX14 3EA, UK.

January 1997

CONTENTS

SUMMARY

Reliability and life predictions are major issues for the critical JET Neutral Beam components during the DTE1 experiment and possible upgraded injection scenarios. Neutral Injection (NI) upgrades may result in an increase of the thermal loads, by at least 20%, to their maximum value.

Reliability prediction under thermal loads is quite complex because in addition to normal stress and fatigue calculations, (boiling) heat transfer phenomena, burnout, material data at high temperatures and lack of thermal fatigue material measurements may lead easily to very conservative and too restrictive estimates.

An attempt has been made to calculate realistic values of fatigue life for the critical JET components: PINI grids, backpanels, hypervapotrons and Duct Scrapers. Boiling heat transfer calculations under the maximum thermal loads predicted the temperature fields and then F.E analyses gave the predicted strains. The latter are relatively high but if one considers the secondary nature of the thermal loads, these high values can be accepted by the codes. In addition, material data incorporating complex phenomena like hardening and ageing result in realistic life predictions.

Cu, CuCrZr and CuNiSi have been extensively used in the JET NI equipment. These materials are also expected to be used in Next Step Devices. Fatigue and fracture properties of these materials at room and elevated temperatures have been obtained in addition to usual tensile data in order to assess the reliability of the equipment. It has been demonstrated that the Manson formula for predicting fatigue initiation based on tensile data can be used. It is also shown that ageing of the material may result in increase in fatigue life for a specified strain value despite the reduction in yield and ultimate strength. This is due to crystalline changes in the material structure which may result in material softening, reduction of the Young's Modulus and increase of the ultimate material elongation.

In addition, other material properties like thermal conductivity and electrical resistivity over a very wide range of temperatures have also been investigated. It has been shown that these Cu alloys demonstrate, over a wide temperature range and under relatively high thermal loads of up to 12MW/m^2, good thermal conductivity, relatively high electrical resistivity, high strength, high fracture toughness and long fatigue life.

Based on the above analyses it was concluded with adequate safety margin that the remaining life of the critical components is adequately long both for DTE1 operation and for extended upgraded injection scenarios.

1. INTRODUCTION

Reliability and life prediction for components under relatively high thermal loads depend on the ability to predict thermal strain based on experimental or computed temperature fields and on

realistic material thermal fatigue data. Experimental temperature measurements are usually not detailed enough to generate comprehensive strain fields. In addition, temperature predictions with configurations subject to high heat fluxes and boiling phenomena are difficult due to lack of accurate boiling heat transfer co-efficients applicable to a variety of geometries and lack of burnout limits. Furthermore, it is common that in heat transfer devices, there are total power limits which are rather difficult to calculate because the exact dependence of the heat transfer co-efficient on the bulk temperature of the fluid, or the amount of gas that has boiled off are not well established.

Material thermal fatigue data are also not usually well known; while phenomena like strain hardening, grain size effects, precipitation hardening, specimen size effects, thermal load dynamics and the probabilistic nature of fatigue will affect greatly the life of a component and are difficult to account for.

In this paper an attempt is made to predict realistic values of reliability and life for critical JET NI components under high thermal loads with cooling fluids (water) sometimes in the boiling regime. These components have up to now seen approximately 10^4 cycles.

The predicted temperatures result in relatively high thermal strains well above the endurance limit, but in view of the small primary strain (due only to pressure) and the thermal fatigue behaviour of the material, a relatively large (10^4 - $2 \cdot 10^4$) number of full upgraded power thermal cycles can be allowed. The thermal fatigue behaviour of the materials is usually predicted by applying the Manson formula which is based on constant slopes of logarithmic elastic and plastic fatigue lines and on material tensile data (Appendix 1).

It should be noted that where the primary load is relatively small compared to the material yield strength, thermal stresses of up to double the yield strength (based on a linear calculation) can be accepted. In this case, even if the material operates beyond the yield point, shakedown conditions prevail and the material stress can be accepted provided a proper fatigue assessment is made (Bree diagram, section 2.1).

Finally, in all cases analysed new material data has been used (Appendix 3) and the allowable maximum temperature is less than half of the melting temperature in order to avoid creep phenomena (time dependent deformation under steady load).

2. COMPONENT RELIABILITY AND LIFE PREDICTION

2.1 Hypervapotrons

Figure 1 shows the typical hypervapotron geometry. The JET hypervapotrons have operated reliably for more than a decade with thermal loads of 8 - 10MW/m^2 and with flow velocities of only ~4m/s. Stable nucleus boiling heat transfer regimes result in ability to transfer large thermal loads with relatively low flow velocities and pressure drops [1]. Heat transfer co-efficients in excess of 100 kW/m^{2o}C are common.

Figure 2 gives the predicted thermal load on these elements with an upgraded NI system consisting of 140 kV/60A triode PINIs [2]. It is shown that the calculated loads are at least 20% higher than present operating regimes [3]. The total power on the ~1000mm long element is ~0.87MW.

C. Baxi [4] has developed a model to predict temperature gradients for hypervapotrons. This simulation is unique, accounting successfully for the boiling heat transfer.

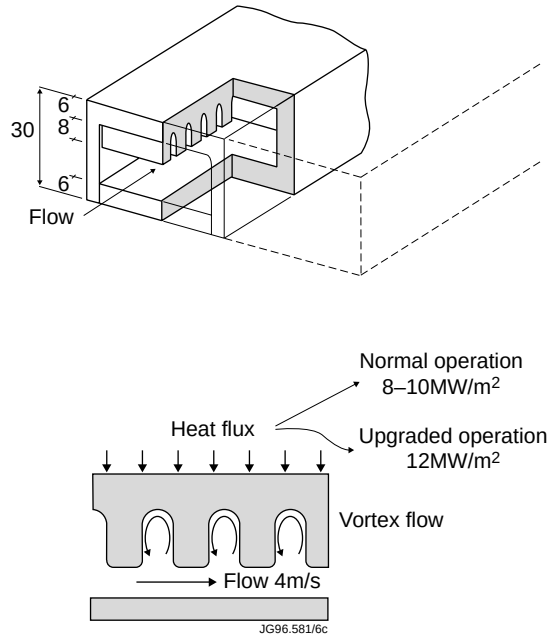

Fig.1: Typical Hypervapotron Geometry.

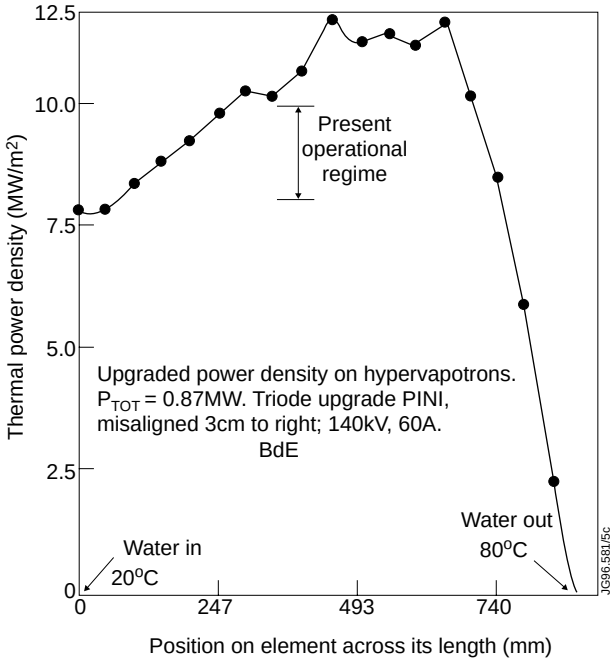

Fig.2: Predicted Thermal load on Hypervapotrons with Upgraded Injection Scenarios.

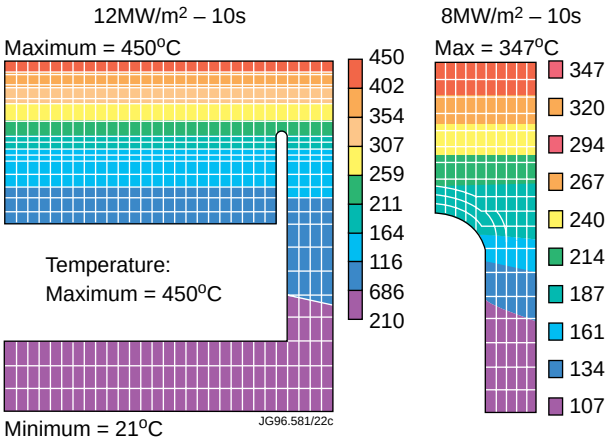

Fig.3: Predicted Typical Fin Temperature Gradient for Hypervapotrons.

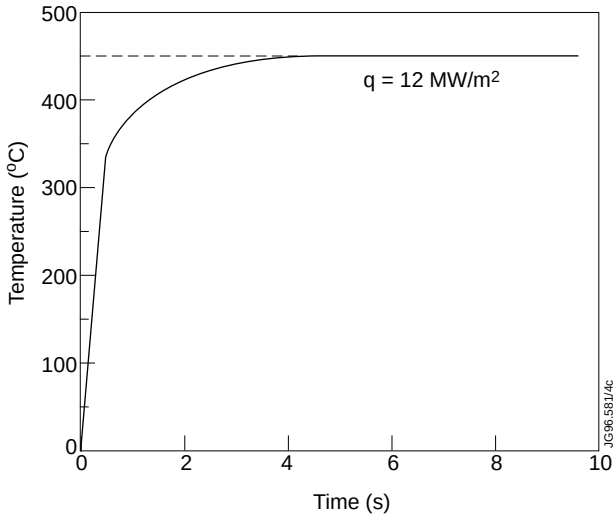

Fig.4: Time Dependent Calculations of Maximum Temperature Gradients for Hypervapotrons.

Figures 3 and 4 exhibit the calculated temperature-time dependent fields given by this model. In addition, Baxi predicted that the burnout limits of the hypervapotrons are well above 12MW/m^2 and 0.9MW/element, under the JET operating conditions. It should be noted that the

Baxi model is in broad agreement with discrete temperature measurements in locations of the JET hypervapotrons done at the JET Test Bed. [4]

Figure 5 shows the FE models of the JET hypervapotrons [5]. By simulating the whole element and its support, we were able to incorporate accurate boundary conditions in a detailed model of an element cross-section. Figure 6 gives the time dependent stress prediction of the hypervapotron for the 140kV/60A triode PINI beam load of 12MW/m^2. It is of particular note that the peak stress in the material occurs at relatively short times (0.4 - 0.6s). This is important, because it indicates that short pulses (traditionally used for 'conditioning' of the high voltage sources) are, in this respect more challenging than the long pulse steady-state cases which have previously been studied. The fact that maximum stresses occur very early in the thermal cycle can be explained by the heat transfer time constant of the hypervapotrons. This is given by the Fourier parameter $t=\ell^2/a$; where ℓ is the element characteristic length, 6mm, and a is the material thermal diffusivity; $t \cong 0.4$s. This time characterises the duration of the thermal wave to reach the rear face of the element front wall and generate large temperature gradients. After this time, boiling heat transfer starts to dominate the phenomena and relieves the stresses. This effect is clearly shown also in figure 4. Until approximately 0.4-0.6s, the temperature increase is linear and follows the simple conduction law. At longer periods, temperature gradients curve due to convection and then boiling heat transfer to water.

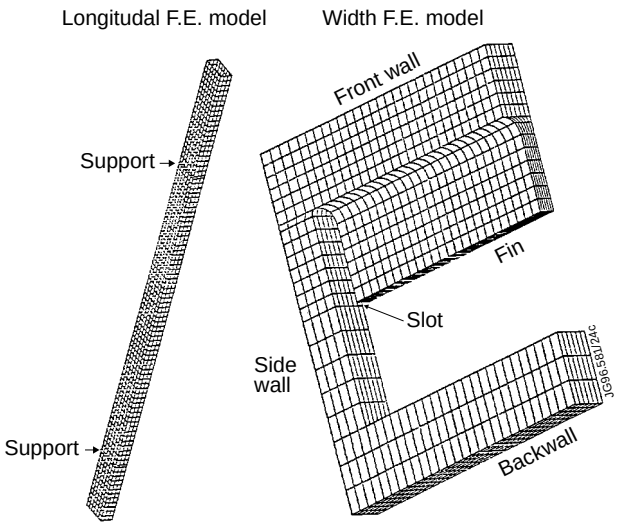

Fig.5: Finite Element Models of the JET Hypervapotrons.

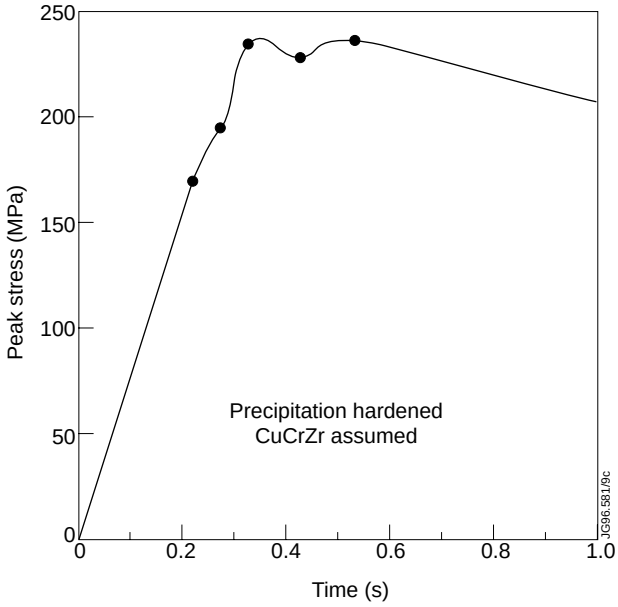

Fig.6: Time Dependent Stress Prediction of Hypervapotrons with 12MW/m^2

Figure 7 exhibits stress and temperature predictions of hypervapotrons for 10MW/m^2[6].These last calculations were performed more than a decade ago and although they are rather pessimistic (with respect mainly to temperature fields), they are in broad agreement with the present analysis. However, at the time of this prediction, no accurate fatigue life calculations were made due to lack of material data.

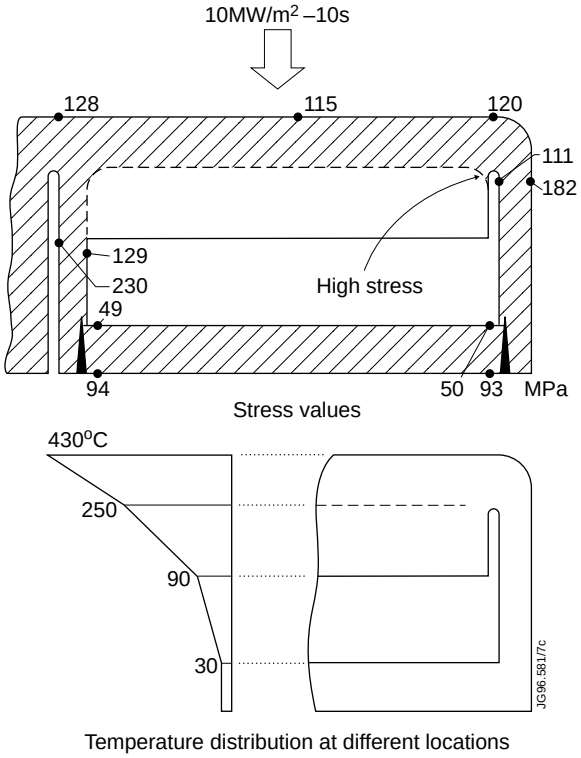

Fig.7: Hypervapotron Temperature Profiles and Stresses under 10MW/m^2, R Haange [6] - 1984.

Hypervapotrons are made from precipitation hardened CuCrZr. The effect of material hardening at 475^{o}C for 3 hours and ageing at 650^{o}C for 1 hour has been quantified [7]. Tensile data for both conditions have been measured. From specimen cut-outs from used elements, it was clear that the material is indicating strong signs of ageing. The measured tensile behaviour is much closer to aged condition. Aged CuCrZr has reduced ultimate tensile strength, yield strength and relatively low Young's Modulus. However, it is rather softer than hardened material with longer ultimate elongation, due perhaps to gradual relaxation of residual stresses at temperature. These residual stresses are generated during the precipitation hardening process. Figure 8 exhibits schematically the possibility of aged material having longer fatigue life than hardened one.

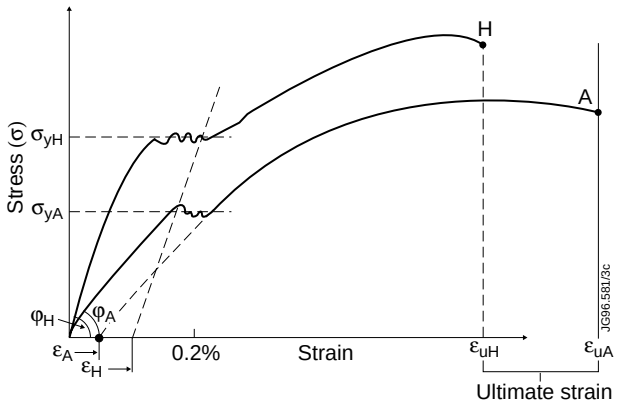

H	Hardened	Material
A	Aged	
ε_A	Strain after removal of stress for aged material	
ε_H	Strain after removal of stress for hardened material	
tan φ_A	Young's Modulus (Aged) – E_A	
tan φ_H	Young's Modulus (Hardened) – E_H	

Typical values for CuCrZr at 450^{o}C

	H	A
σ_y (MPa)	200	140
σ_u (MPa)	250	190
ε_u %	22	31.5
E (GPa)	100	70

Fig.8: Schema exhibiting the Cyclic Behaviour of Hardened and Aged Material.

CuCrZr

	Hardened	**Aged**
Yield Strength (MPa)	200	140
Ultimate Strength (MPa)	250	190
Young's Modulus (GPa)	100	70
Ultimate Elongation %	22	31.5

Table 1 High temperature material properties for aged and hardened CuCrZr

This effect is mainly based on the combination of reduced Young's Modulus and increased ultimate elongation. Table 1 shows typical values of yield, ultimate strength, ultimate elongation and Young's Modulus for hardened and aged CuCrZr.

Table 1 indicates that the predicted element stresses (fig 6) are rather high. However, they are accepted by ASME, particularly if one considers the secondary nature of thermal stresses [5]. The Bree diagram [8] shows graphically the acceptance of relatively high thermal stresses. Figure 9 gives the Bree diagram for the hypervapotron behaviour with 12MW/m^2 and different pulse lengths. It is clear that although the hypervapotrons operate in non-linear regimes, these are in shakedown regions and can be accepted. (See Appendix 2) [5].

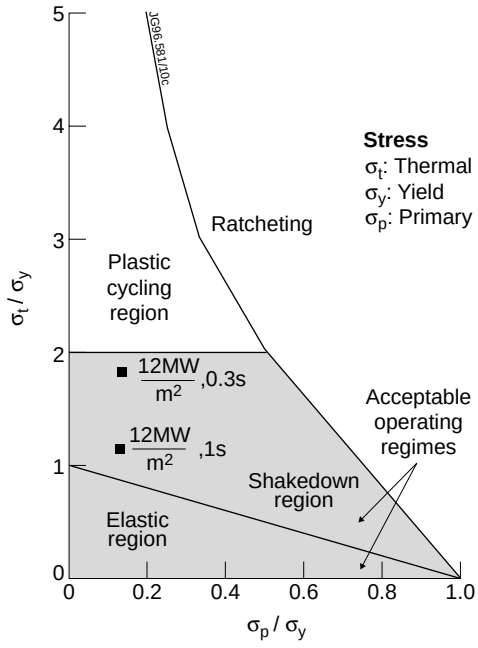

Fig.9: Hypervapotron Bree Diagram.

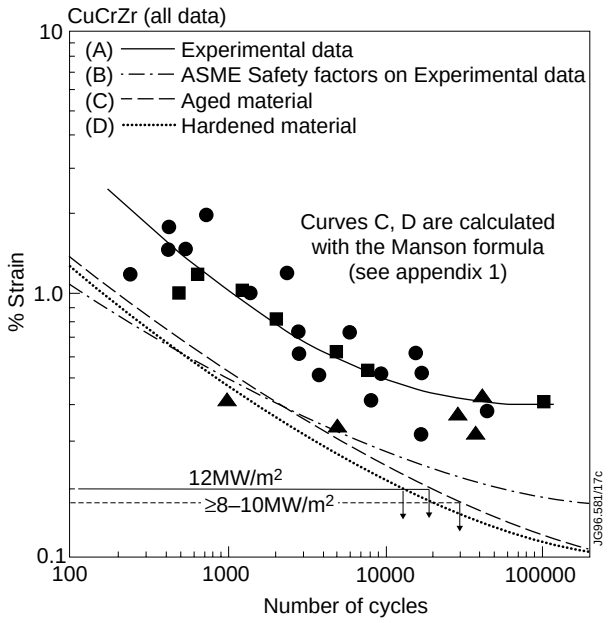

Fig.10: Fatigue Curves for CuCrZr.

Figure 10 shows 4 typical fatigue curves for CuCrZr. Curve A gives the JET experimental data of push-pull mechanical tests. Curve B applies typical safety factors of cycles /10 and strain/2 to curve A. Curves C and D are predicted fatigue curves based on tensile data and the

Manson method [5], [9] (See Appendix 1) for aged and hardened conditions respectively. The Manson method gives low bound predictions for fatigue life of CuCrZr.

The maximum predicted strain for 12MW/m^2 is ~ 0.4% [5]. Since the minimum strain is 0, the absolute half strain amplitude is 0.2%. From Figure 10 and the Manson curves (C, D) one can predict 13000 to 20000 permitted cycles under 12MW/m^2 for hardened and aged material respectively. However the cycles today, under 8 - 10MW/m^2 are ~ 10^4. At these power levels the maximum strain is ≤ 0.36%. This value is obtained, assuming an average maximum temperature for 8 - 10MW/m^2, of ≤ 400°C, figure 3. Since the maximum temperature for 12MW/m2 is ~ 450°C and as a first order of approximation, the strain is proportional to temperature gradients, one obtains a maximum strain of $\frac{400}{450}$ 0.4% $\simeq$ 0.36%. From Figure 10 we can predict 20000 to 30000 permitted cycles under 8 - 10MW/m^2 for hardened and aged material respectively.

The Miner's/Paris rule for cumulative cyclic loads which vary in magnitude is $\sum \frac{n_i}{N_i} = 1$, where

n_i numbers of cycles seen at a particular strain level,

N_i: number of permitted cycles at same strain level.

Hence for hardened material we predict

$$\frac{10^4}{2.10^4} + \frac{x}{1.3\ 10^4} = 1 \Rightarrow \quad x \approx 6500 \ \text{ cycles}$$

for aged material:

$$\frac{10^4}{3\ 10^4} + \frac{y}{2\ 10^4} = 1 \ \Rightarrow y \cong 14000 \ \text{ cycles}$$

Therefore the remaining material life under 12MW/m^2 is 6500 to 14000 cycles depending on whether the material is hardened or aged respectively. Considering that the material is rather aged **we predict that we can still operate for another 14000 cycles with considerable safety**. This is because figure 10 demonstrates that the Manson formula for predicting fatigue life is rather a conservative assumption compared to our material measurements at room temperature, even if we incorporate the ASME safety factors to account for temperature effects.

In addition it should be noted that curve A (Figure10), which refers to axial fatigue, is usually a very conservative approach to bending fatigue. This is due principally because specimen size effects are very significant in bending fatigue since the peak stress is concentrated in outer fibres, while in axial fatigue the stresses do not vary in the cross-section. Thus the possibility of material imperfections which may initiate fatigue is larger in axial tests. It is therefore concluded that the use of the most conservative curves in figure10 for fatigue assessment purposes, gives a relatively high safety margin for reliability and life prediction.

The above analysis uses half of the maximum oscillating strain/stress to calculate life cycles. This is normal practice in fatigue assessment when the minimum value of the oscillating strain is zero. In addition to this, the Gerber relationship [5,10] attempts also to assess safe or

unsafe operating regimes for an oscillating stress with any minimum value. The safe regime is distinguished by the unsafe one, from a curve given by the formula

$$\sigma_a = \sigma_f \left[1 - \left(\frac{\sigma_m}{\sigma_{ts}} \right)^2 \right]$$

where σ_a : fatigue strength in terms of stress applied when $\sigma_m \neq 0$, figure11

σ_m : mean stress

σ_f : fatigue strength in terms of stress applied when $\sigma_m = 0$

σ_{ts} : tensile strength, figures 20, 21.

In addition σ_f = e E, where E is the Young's Modulus at temperature, figure 22; e is the strain level for a certain number of cycles and a specific fatigue curve, figure10.

For aged material and 2.10^4 cycles, $\sigma_f \cong \frac{0.4\%}{2}$ 70 GPa = 140 MPa

For hardened material and 1.3 10^4 cycles $s_f = 0.18\%$ 100 GPa = 180 MPa.

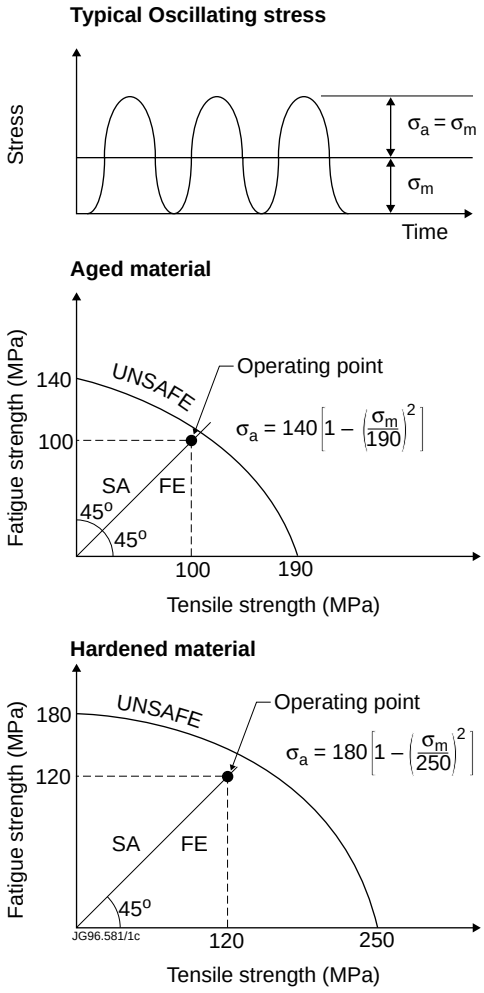

Fig.11: Effect of Mean Cyclic Stress on Hypervapotron Fatigue Behaviour, according to Gerber.

Note that the mean values of Young's Modulus and tensile stength at 450^{o}C are taken from figures 20, 21, 22. These figures depict also the low bound values of E, σ_{ts} and their relationship with temperature. The use however of the lowest values of E in fatigue calculations may result in optimistic estimates.

The operating point for the hardened material is on a 45° line ($\sigma_{m} = \sigma_{a}$) figure11, and, from figure 6, at a stress level of σ= 240/2 = 120 MPa. This point lies in the safe regime. **Similarly the operating point for the aged material lies also in the safe regime.**

The above analysis attempts to quantify the effect of $\sigma_{m} \neq 0$. It is of particular importance in cases with $\sigma_{m} >> 0$, since, in these loading conditions, one would not simply use only σ_{a}, figure 11, for fatigue/reliability asdsessment purposes, figure 10; section 2.2. The use of the Gerber relationship, as compared to other more conservative formulae (Goodman, Soderberg) [10] is fully acceptable because the Manson formula, for predicting fatigue is itself conservative enough, fig.10. Otherwise one can end up with too restrictive rather unrealistic predictions.

2.2 PINI backpanels

Figure 12 gives a detail of a PINI backpanel. OFHC Cu is brazed on a stainless steel backplate. The power density for upgraded 140kV/60A PINIs is ~4MW/m^{2} [2], while the flow velocity in the water cooling channels is ~8m/s. These elements were originally designed for much lower power densities and for forced convection cooling. The forced convection co-efficient is ~28kW/m^{2o}C.

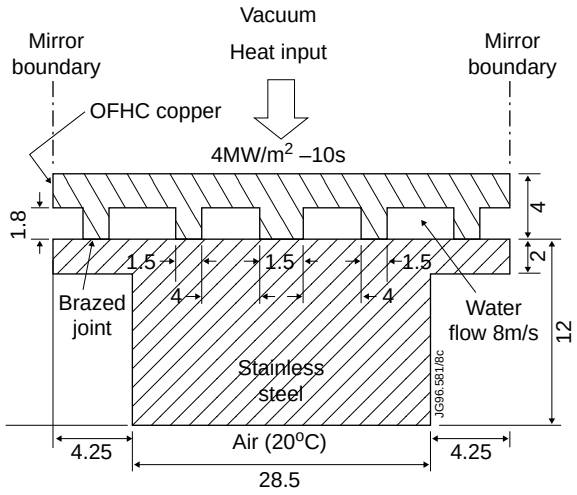

Fig.12: Detail of PINI Backpanel.

FE models were applied to predict the temperature and strain fields of these elements. PINI backpanels would operate in the limit of forced convection heat transfer under 4MW/m^{2} . Should some nucleus boiling occur, the heat transfer co-efficient would increase and the strain and temperature fields decrease. A moderate 30% increase in the heat transfer co-efficient would result in 15% reduction in maximum temperatures and 20% reduction in strain. Provided that the burnout limits are not approached, some boiling heat transfer is therefore beneficial. Figures 13 and 14 show predicted temperatures and strains respectively for these elements with 4MW/m^{2} under forced convection (conservative assumption). The predicted strain cycles in figure 14 are not identical due to (mainly) numerical effects in the calculations. However within the anticipated accuracy of a strain analysis they are accepted as equal. The elements originally deform with a maximum 0.4% strain and then oscillate over a range around ~0.1% strain. Fatigue life is therefore determined only by this 0.1% strain.

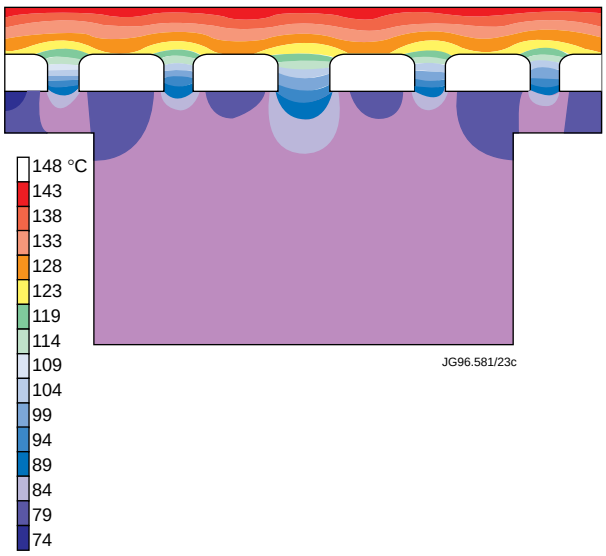

Fig.13: Predicted Temperatures of a PINI Backpanel with 4MW/m^2.

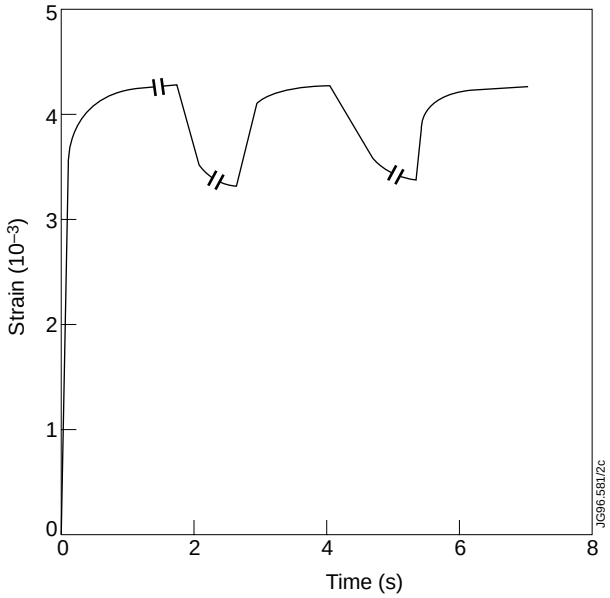

Fig.14: Predicted maximum strain of a PINI Backpanel with 4MW/m^2.

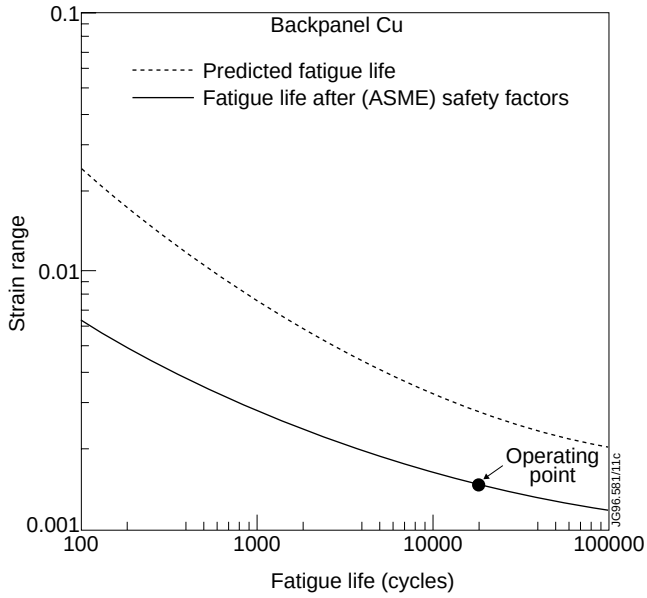

Fig.15: Fatigue Behaviour of PINI Backpanels.

Figure 15 gives **the predicted behaviour (~20000 cycles) of PINI backpanels** with 4MW/m^2. The predicted fatigue curve is based on the Manson formula [9], see Appendix 1.

2.3 PINI grids No. 1

Figures 16 and 17 exhibit the PINI grid 1 geometry and the FE model used to predict the thermal stress behaviour of these elements. The maximum power density for upgraded NI scenarios is ~2MW/m^2 , while the total power handled by this element is ~66KW. The predicted maximum temperatures are ~72^{o}C. The maximum stresses depend on the assumed boundary conditions of

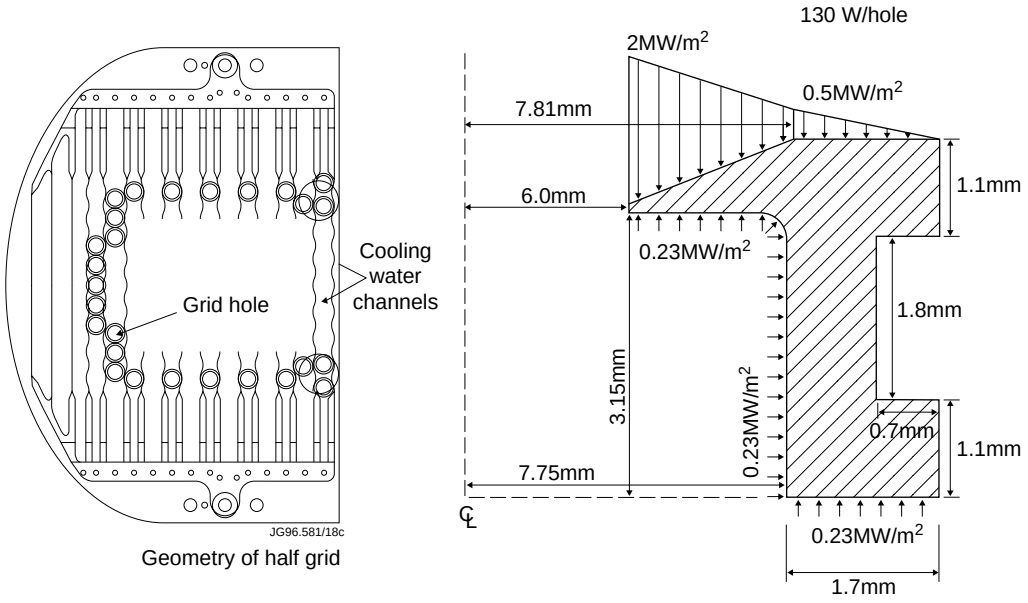

Fig.16: Geometry of PINI Grid 1.

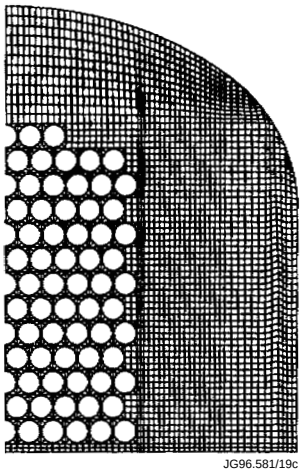

Fig.17: FE Model of PINI Grid.

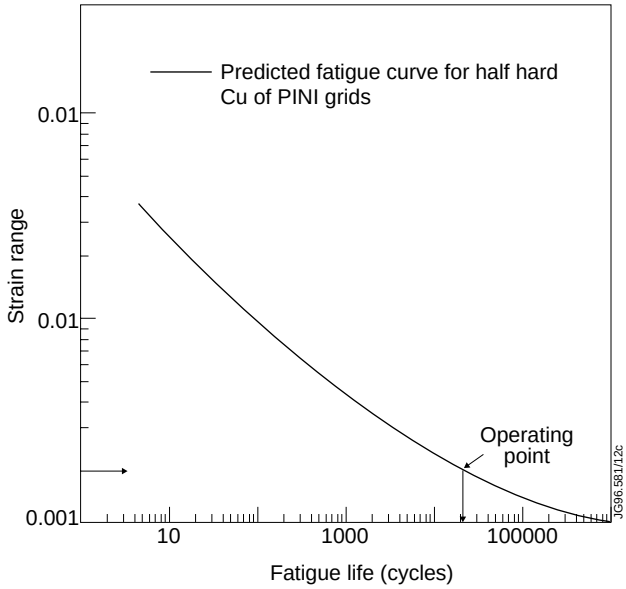

Fig.18: Fatigue Life of PINI Grid 1.

the simulated critical grid hole detail. For a maximum 2MW/m^2 and power loss of 130W/hole, the predicted maximum (conservative) stresses are ~270MPa. This value is rather close to the limits of the ASME acceptance criteria. However, figure 18 gives the predicted fatigue life of the Cu used. It is shown that taking into account the Young's Modulus, **one can accept up to 20000 cycles.**

The critical Cu, stainless steel interface sees mainly compressive stresses and therefore the (rather unknown) quality of brazing in this area is not critical.

Further to this conservative life prediction, mechanical fatigue tests were carried out. Test pieces were cut out from used grids and were cycled on a 3-point bending machine. **The applied strain was larger than the calculated one and yet the samples did not show any signs of**

cracking after 50000 cycles. It was again concluded that the Manson formula for predicting fatigue life was a low bound conservative calculation.

In addition to the work referred to in this report, further analysis has also been done to investigate grid deflections and membrane stresses due to grid supports **[11]**. Prediction of grid deflections with ANSYS (used in this report) agreed with estimates with COSMOS (used by D. Martin) [11]. However membrane stresses due to grid supports are not accounted in this report since this would have required an excesively large/expensive FE model to make accurate predictions. For this reason the mechanical fatigue experiments done were at higher stress levels.

2.4 Duct Scrapers

Figure 19 indicates a JET NI Duct Scraper. Cu plates of various thicknesses line the JET inconel walls to accommodate beam scraping and reionised power loadings. The inconel duct walls can take up to 0.5MW/m^2 or 1MW/m^2 for only 1000 cycles; while power densities in excess of 7 to 8MW/m^2 are expected in the Duct region. The Duct Scraper is cooled, unlike the other actively cooled components, by inter-pulse water or radiation cooling.

FE models were applied to predict the temperature and stress fields of the copper tiles, as before. **For approximately 10000 cycles** it was found that **the limiting factor is the maximum tile temperature (500^{o}C)** in order to avoid creep and considerable degradation of material properties. **Provided such a temperature limit is observed, the ASME limits are satisfied. [12]**

This analysis accounts for thermal loads only. The Duct Scrapers, however, see also considerable disruption loads of up to 100T/s. The Cu tiles are mounted on the Duct Scraper in such a way as to minimise the generated eddy current stresses. **[13]**

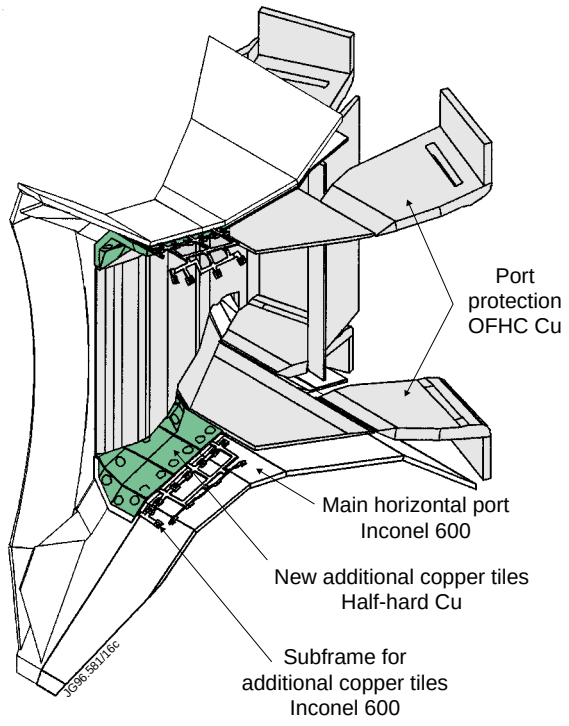

Fig.19: The JET NI Duct Scraper.

2.5 Validation of Calculations

Although direct thermal strain measurements are rather difficult and have not been attempted as such, there is a high level of confidence in the life predictions of this report. With respect to hypervapotrons, independent stress analyses (figures 6,7) agreed well in predicting maximum values while temperature calculations were in line with measurement at the JET Test Bed [4]. In

PINI grids, independent deflection calculations with two commercial programs (ANSYS, COSMOS) agreed well, while experimental evidence confirmed our (conservative) predictions. In PINI backpanels and Duct Scrapers, the use of a well established commercial FE program (ANSYS) together with conservative assumptions in heat transfer resulted in confidence in the conclusions of the analysis.

Finally the use of the Manson formula to determine fatigue initiation has been proven to be a safe, rather conservative, calculation (figure 10; section 2.3) when it is compared with material experimental data.

3 CONCLUSIONS

The critical NI components have operated for $\leq 10^4$ cycles over the past decade. In this report they have been analysed in order to calculate their reliability and estimate the expected remaining life in view of the DTE1 experiment, and possible enhanced injection scenarios. Realistic material data at temperature, together with phenomena like ageing, and hardening have been accounted. Experimental and analytical fatigue data have been used together with extensive FE calculations to predict stress/strain levels.

In all cases the predicted remaining life cycles were well in excess of 10^4 with considerable safety margins.

ACKNOWLEDGEMENTS

The author wishes to acknowledge the contribution to this report of P Ageladarakis, D Starkey, A Lawer from JET, R Tivey from ITER and B Daniels, T Richarson from AEA Technology.

REFERENCES

[1] H Falter, E Thompson: Performance of Hypervapotron Beam Stopping Elements in JET; JET-P(95)13.

[2] EUR FU 96/JET-SC 54/6.3.

[3] H P L De Esch; Personal Communication; JET 1996.

[4] C Baxi, H Falter; A Model for Analytical Performance Prediction of Hypervapotrons; JET-P(92)56.

[5] B D Daniels, et al; JET Hypervapotrons - Assessment of short Commissioning Pulses, AEA Technology Report SPD/D(96)612, August 1996.

[6] R Haange; Components for the Neutral Injection Beamlines; Mechanical Engineering Aspects of the JET Fusion Project; Inst of Mech Eng, London, Nov 1984.

[7] R Tivey; Personal Communication; ITER; Garching 1995.

[8] J Bree; Elastic-Plastic Behaviour of Thin Tubes Subjected to Internal Pressure and

Intermittent High-Heat Fluxes with application to Fast Nuclear Reactor Fuel Elements; Journal of Strain Analysis, Vol 2, p 226 ,(1967).

[9] S Manson, G L Halford; A Method of Estimating High Temperature, Low Cycle Fatigue Behaviour of Materials, proc. of International Conf. on Thermal and High Strain Fatigue, Metals and Metallurgy Trust, London (1967), 154.

[10] R W Hertzberg; Deformation and Fracture Mechanics of Engineering Materials, 3rd Edition; Wiley 1989.

[11] D Martin: Personnal Communication; to be published; JET, 1997

[12] B D Daniels, et al; Structural Integrity Assessment of the JET Duct Scraper, AEA Technology Report SPD/D(95)460; November 1995.

[13] S Papastergiou, P Ageladarakis; Optimisation of Support Positions for Fusion In-Vessel Components to Minimise Eddy Current Stresses; submitted to Fusion Engineering and Design; to appear.

[14] S Papastergiou, et al; Materials Selection Qualification and Manufacturing of the In-Vessel Cryopump for JET, Advances in Cryogenic Engineering, 1993, Vol 40, 1429.

[15] P Ageladarakis; Aspects of Operational Safety and Mechanical Integrity of the Cryopump System in the JET Fusion Tokamak, PhD Thesis, Imperial College, London 1996.

[16] ASME III Division 1 - Sub-section NB Classs 1 Components, 1992 Edition.

[17] D R Miller; Thermal-Stress Ratchet Mechanism in Pressure Vessels, Transactions ASME, Vol 81, p 190 (1959).

[18] S Papastergiou et al; Operational Safety of the JET In-Vessel Divertor Cryopump; 18th Fusion Technology Conference proc., 1994, Karlsruhe, Germany.

[19] S Papastergiou et al; Effects of High Frequency Disruptions on the JET Divertor Cryopump; 19th Fusion Technology Conference proc., 1996, Lisbon, Portugal.

APPENDIX 1

THE MANSON FORMULA FOR PREDICTING FATIGUE LIFE

Fatigue data can be predicted by using the material tensile behaviour. This has been demonstrated by Manson [9] and proven also, by our own Cu and CuCrZr fatigue measurements (Fig 10) to be a rather conservative/safe calculation.

The formula depicting the material fatigue behaviour is:

$$\Delta e = \left[\frac{3.5 \times \sigma_u}{E} \times N_f^{-0.12}\right] + \left[D^{0.6} \times N_f^{-0.6}\right]$$

where: Δe is total strain range

N_f is number of cycles to fatigue

D is true tensile ductility

σ_u is ultimate tensile strength

E is modulus of elasticity

and $$D = 1n\left[\frac{100}{100 - RA}\right]$$

where: RA is percentage reduction in area.

This method is based on the experimentally proven assumption over a very wide range of materials that the slopes of the elastic and plastic fatigue lines in a logarithmic scale are constant. The two main variables governing the phenomenon are the ultimate tensile strength and area reduction during tensile tests. Yield stress is a property of little importance because strain hardening or softening under cyclic stress modifies the originally stress-strain curve of the virgin material. In addition, fracture toughness does not also play an important role due to the fact that the Manson method refers mainly to fatigue initiation and until this stage, the material fracture resistance does not influence life.

The Manson formula can be applied directly without adjustment to materials below the creep temperature range (half of melting temperature). The components analysed in this report operate just below this temperature limit.

APPENDIX 2 (REF 5)

ASME STRESS ASSESSMENT REQUIREMENTS

2.1 Elastic Stress Limits

The stress limit assessments have been performed, in-line with the ASME philosophy, to check the overall stress levels. The design stress intensity value (Sm) is the least of either one-third of the ultimate tensile strength (σ_u) at temperature or two-thirds of the yield strength at temperature (σ_y). The thermal stresses have been classified using the ASME III classifications as secondary stress (ie self-limiting). Local yielding and minor distortion can satisfy the conditions (ie shake-down) which cause the stress to occur but failure from one application of the stress is not expected. The assessment stresses are compared below to the ASME III stress limits for design and Level-A service requirements for class 1 components.

Pl	$\leq$ 1.5 Sm
Pl + Pb	$\leq$ 1.5 Sm
Pe	$\leq$ 3 Sm
Pl + Pb + Pe + Q	$\leq$ 3 Sm
Pl + Pb + Pe + Q + F	$\leq$ 2 Sa

Where: Pl is local primary membrane stress due to pressure
Pb is primary bending stress due to pressure
Pe is thermal membrane stress
Q is secondary stress due to thermal loads
F is peak stress due to stress concentration effects
Sm is design stress intensity (lesser of 0.33 σu or 0.66 σy)
Sa is allowable stress amplitude for an acceptable number of cycles

2.2 Simplified Elastic-Plastic Limits

The elastic stress limit (3 Sm) on the primary plus secondary stress may be exceeded provided that the following requirements are met:

1) The range of primary plus secondary membrane plus primary bending (Sn), excluding thermal bending stress, must be less than or equal to 3 Sm.

2) The stress amplitude (Sa) used for entering the design fatigue curve is multiplied by the factor Ke, where:

$Ke = 1$ for $Sn \leq 3\ Sm$

$$Ke = 1 + \left(\left[\frac{1-n}{n(m-1)} \right] x \left(\frac{Sn}{3Sm} - 1 \right) \right) \quad \text{for } 3\ Sm < Sn < 3\ m\ Sm$$

$$Ke = \frac{1}{n} \quad \text{for } Sn \geq 3\ m\ Sm$$

where: Sn' is range of primary plus secondary stress (ie excluding peak stress)

Note: In absence of values for copper material, it has been assumed that 'm = 1.7' and 'n = 0.3' (ie Nickel-copper in Table NB-3228.5 (b)-1 of Reference 16)

3) No thermal ratcheting (ie elastic strain limits).

4) The material should have a specified minimum yield strength to specified minimum tensile strength ratio of less than 0.80 (ASME definition of ductile material). Using the tensile properties (section 2.3) for the hardened and the aged materials, the tensile strength ratio's are 0.82 and 0.76 respectively for CuCrZr.

2.3 Elastic Strain Limits

The incremental growth of a component subjected to mechanical loading with superimposed thermal cycles may lead to distortion or fracture unless the accumulated inelastic strain is kept within allowable limits. The interactive effect of the thermal cycles on the stress distribution within components can be evaluated using the uniaxial model originally proposed by Miller [17] for elastic-plastic behaviour, and redefined by Bree [8] for cyclic load histories. Bree criteria limit mechanical and thermal stresses to eliminate component incremental growth of strain.

The Bree model is based on the assumption that although high temperature causes the resulting stress field to relax, each thermal cycle subsequent to the relaxation period re-institutes the original elastic-plastic stress distribution. For shakedown or plastic cycling to exist, a portion of the wall thickness must remain elastic throughout the life of the component (ie elastic core). The stress history of the elastic core can conveniently be used to bound inelastic strains accumulated through the wall of the component. The short-term redistribution of stress in the elastic core during the transient does not affect the accumulation of inelastic strain, and can therefore simply be disregarded.

The accumulated inelastic strains can be bounded, using the results of elastic analysis and the following simple relations are derived from equilibrium considerations (ie Bree diagram, figure 9). Typical stress profiles for characteristic combinations of mechanical stress (σ_p) and cyclic thermal stress (σ_t) are related to the yield stress (σ_y):

$\sigma_y = \sigma_p + \sigma_t$	Elastic region
$2 \times \sigma_y = \sigma_t$	Shakedown region
$\sigma_y = \sigma_p + (0.25 \times \sigma_t)$	Shakedown region
$\sigma_y^2 = \sigma_p \times \sigma_t$	Plastic cycle region

In many applications it is not feasible to keep all elastically calculated stresses less than the yield strength. In such components, plastic cycling can be allowed, provided that both effects can be limited and kept within safe allowable values, shown in the Bree diagram (Fig 9). The ratcheting region indicates the potential exhaustion of the material ductility and fatigue failure in fewer cycles than may be indicated by fatigue assessment. The thermal ratcheting requirements in ASME design code are based on the BREE diagram.

APPENDIX 3

MATERIAL DATA

3.1 Cu

OFHC Cu in annealed or half hard condition has been used in the Duct Scrapers and PINI backpanels. Annealed OFHC copper exhibits cyclic strain hardening prior to reaching cyclic strain stability, while relatively hard copper may show strain softening (Bauschinger effect). The JET material is believed to exhibit some (beneficial) cyclic strain hardening (Duct Scrapers) but usually to be stable and certainly to avoid the detrimental Bauschinger effect. The half hard copper used in the radiation cooled Duct Scraper tiles and PINI backpanels has relatively large dislocation density (crystal lattice imperfections) to be relatively hard but not to show strain softening. Its yield strength varies from 215 to 297 MPa, while the ultimate strength varies from 235 MPa to 300 MPa respectively. Typical fatigue lifes are given in figures 15 and 18.

3.2 CuCrZr

Precipitation hardened CuCrZr is used in the JET hypervapotrons. This alloy is heated to 475^{o}C for several hours and then quickly quenched so that no new crystal phases appear and its strength remains rather high (Table 1). If during operation, this alloy reaches relatively high temperatures this new (previously avoided) crystal phase appears in the grain boundaries, the material ages and its strength reduces. However, the material becomes also softer, its ultimate elongation increases and the Young's Modulus reduces. This may lead to an increase in fatigue life (fig 8).

Figures 20, 21 and 22 show the temperature relationship of yield, ultimate strength and Young's Modulus and the low bound temperature dependence, according to the condition of CuCrZr.

Figure 10 gives typical fatigue curves for this material.

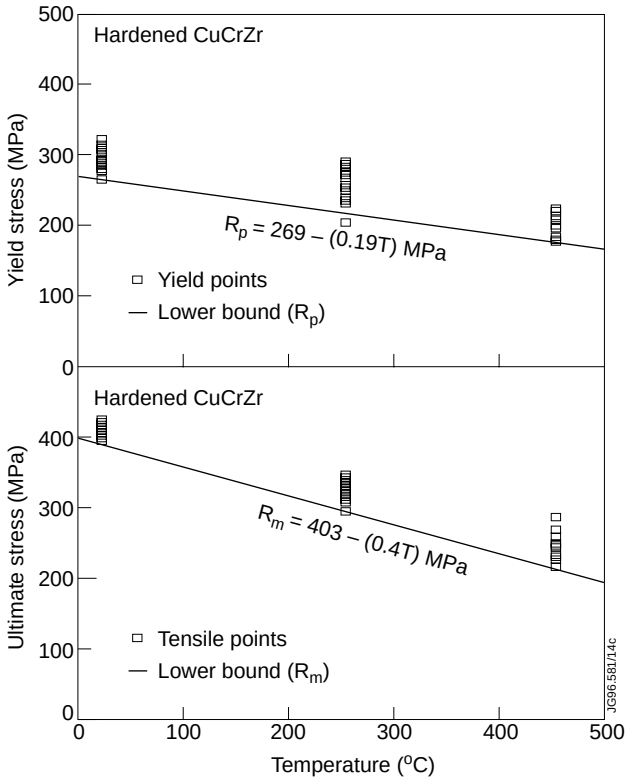

Fig.20: Yield and Ultimate Strength of Hardened CuCrZr.

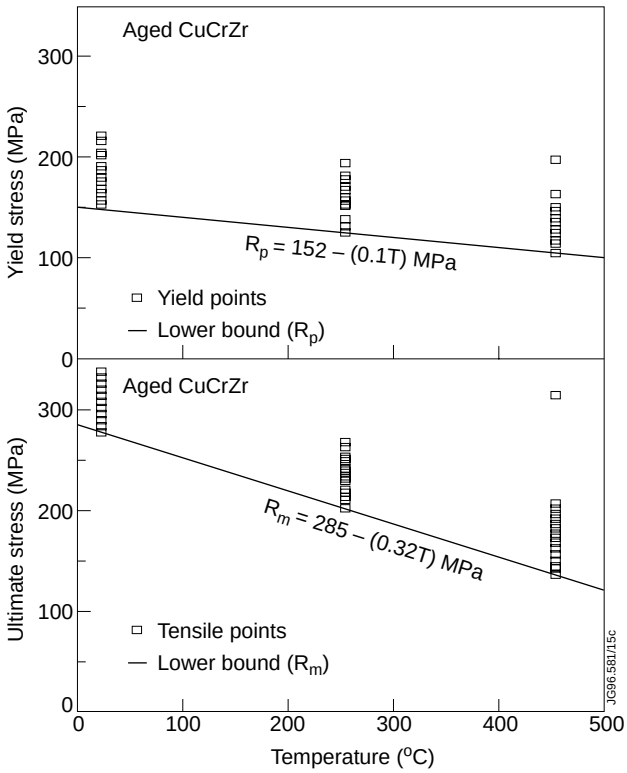

Fig.21: Yield and Ultimate Strength of Aged CuCrZr.

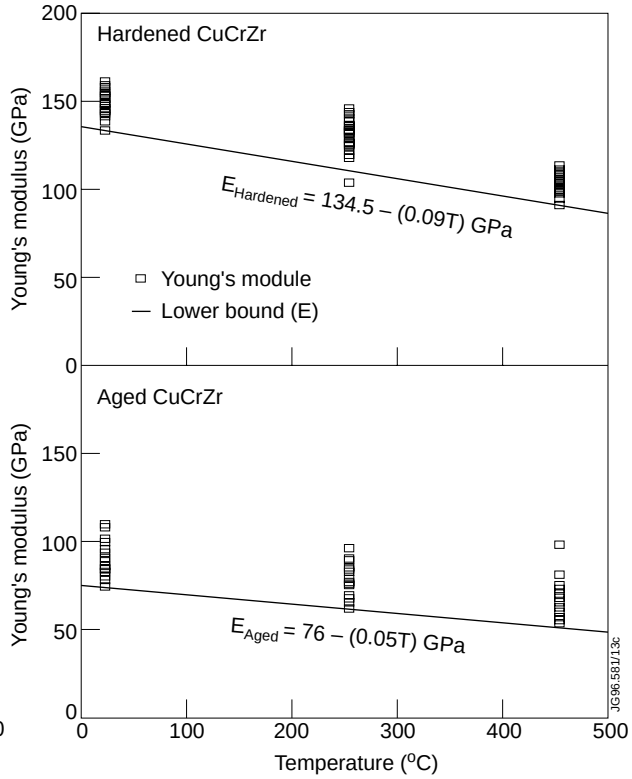

Fig.22: Young's Modulus of Hardened and Aged CuCrZr.

3.3 CuNiSi

CuNiSi has been used in the JET Divertor cryopump and baffles. It has been preferred to CuCrZr because its electrical resistivity at cryogenic and ambient temperatures is higher than CuCrZr while its thermal conductivity is still good. These properties result in relatively lower eddy current stresses and adequately low temperature gradients and thermal stresses.

Material	Property	Temperature (K)	Result
CuCrZr	Thermal Conductivity $Wcm^{-1}K^{-1}$	300	3.5
CuNiSi		300	2.2
		77	0.85
CuCrZr	Electrical Resistivity μΩ cm	300	2.42
		77	**0.70**
CuNiSi		300	4.6
		77	**2.9**
CuCrZr	Yield Strength MPa	300	298
		77	306
CuNiSi		300	426
		77	460

Table 2 Material Properties of CuCrZr and CuNiSi

Table 2 gives the material properties (thermal conductivity, electrical resistivity and typical yield strength) of CuCrZr and CuNiSi over a wide temperature range. [14]

Fracture toughness tests of CuNiSi have been performed by P Ageladarakis [15]. The fracture toughness value for the heat treated material [14] is 85MPa$\sqrt{m}$. This value is close to properties of some stainless steels and in combination with the thermal, mechanical and electrical properties of this material, confirms its potential for Next Step applications.

The JET divertor cryopump/baffles are in-accessible and their reliability must be of the highest possible standard. An inspection during the summer of 1995 (last time these components were accessible) showed no identifiable cracks. However, it is of major importance to quantify structurally tolerable crack sizes under the worst service conditions, namely maximum thermal stresses during normal or abnormal conditions [18], or maximum dynamic stresses during disruptions [19]. A theoretical failure by fracture analysis of divertor cryopump/baffles, according to BS and ASME, has been performed [15]. Using the material yield strength and fracture properties, a crack size of up to even 9.6mm can be accepted without leading to component failure. It was shown that these materials can accommodate relatively large cracks provided of course that leaks are not generated.